

# 1 Heating of Jupiter's upper atmosphere above the Great Red Spot

2 J. O'Donoghue<sup>1</sup>, L. Moore<sup>1</sup>, T.S. Stallard<sup>2</sup>, H. Melin<sup>2</sup>

3 <sup>1</sup>Center for Space Physics, Boston University, Boston 02215, USA.

4 <sup>2</sup>Dept. of Physics & Astronomy, University of Leicester, Leicester, LE1 7RH, UK.

5  
6 **Measured upper-atmospheric, mid-to-low latitude temperatures of the giant planets**  
7 **are hundreds of degrees warmer than models based on solar heating alone can**  
8 **explain<sup>1-4</sup>. Modelling studies, focused on additional sources of heating, have been**  
9 **unable to resolve this significant model-data discrepancy. Equatorward transport of**  
10 **energy from the hot auroral regions was expected to heat low latitude regions;**  
11 **instead, models have demonstrated that auroral energy is trapped at high latitudes,**  
12 **a consequence of the strong Coriolis forces on these rapidly rotating planets<sup>3-5</sup>.**  
13 **Wave heating, driven from below, represents another potential source of upper-**  
14 **atmospheric heating, though initial calculations have proven inconclusive at**  
15 **Jupiter, largely due to a lack of observational constraints on wave parameters<sup>6,7</sup>.**  
16 **Here we report that the upper atmosphere above Jupiter's Great Red Spot - the**  
17 **largest storm in the solar system - is hundreds of degrees hotter than anywhere**  
18 **else on the planet. The hotspot, by process of elimination, must be heated from**  
19 **below, and this detection is therefore strong evidence for coupling between**  
20 **Jupiter's lower and upper atmospheres, likely the result of upward propagating**  
21 **acoustic and/or gravity waves. Our results indicate that the lower atmosphere may**  
22 **yet play an important role in resolving the giant planet 'energy crisis'.**

23  
24 On 4 December 2012 (UTC) we observed Jupiter for 9 hours using the SpeX  
25 spectrometer<sup>8</sup> on the NASA Infrared Telescope Facility (IRTF). The spectrometer slit was  
26 aligned along the rotational axis in the north-south direction at local noon. This  
27 arrangement is illustrated in Fig. 1a, which contains a slit-jaw image showing bright auroral  
28 emissions at the poles as well as a localised Great Red Spot (GRS) emission  
29 enhancement at mid-latitudes. Exposures from the instrument in this set-up give  
30 wavelength and intensity information as a function of latitude as shown in Fig. 1b. By  
31 exposing continuously throughout the night, we obtained longitudinal information for most  
32 of the planet (a Jovian day is 9hr 56 min).

33  
34  
35 The spectrum in Fig. 1b shows strong emission features at six wavelengths, which appear  
36 prominently in the auroral regions and wane towards the equator. These are discrete ro-  
37 vibrational emission lines from  $H_3^+$ , a major ion in Jupiter's ionosphere, the charged  
38 (plasma) component of the upper atmosphere. The colour contours highlight the weaker  
39 emissions from this ion across the body of the planet. Far from being a uniform intensity at  
40 low-latitudes, there is a significant intensity enhancement in all of the emission lines within  
41 the 13 - 27° planetocentric latitude range occupied by the spot<sup>9</sup>. As seen in the coloured  
42 contours of Fig. 1b, the  $H_3^+$  emissions are isolated in wavelength, indicating that there is  
43 no continuum reflection of sunlight at red spot latitudes.

44  
45  
46 The ratio between two or more emission lines can be used to derive the temperature of the  
47 emitting ions<sup>10,11</sup>. With the observing geometry used here, such temperatures are  
48 altitudinally-averaged 'column temperatures' of  $H_3^+$ , where the majority of  $H_3^+$  at Jupiter  
49 has been observed to be located between 600 to 1000 km altitude above the 1-bar  
50 pressure level<sup>12</sup>.  $H_3^+$  has been demonstrated to be in quasi-local thermodynamic  
51 equilibrium throughout the majority of Jupiter's upper atmosphere, meaning that derived  
52 temperatures are representative of the co-located ionosphere and (the mostly  $H_2$ )

53 thermosphere<sup>13</sup>. In the Methods section we detail the data reduction techniques and  
54 temperature model fitting procedures, and in Fig. 2 we show two example model fits; only  
55 the strongest, outermost lines are used to fit temperatures, as the central  $H_3^+$  lines are  
56 contaminated by telluric absorption. Note that, even though the  $H_3^+$  peak intensities at the  
57 spot (Fig. 2, left) are lower than those at 45° latitude, this is a result of lower column-  
58 integrated  $H_3^+$  densities at lower latitude. Derived temperatures remain unaffected by the  
59 density differences as they are based entirely on  $H_3^+$  line ratios.

60  
61  
62 The difficulty in explaining the observed upper-atmospheric temperatures at the giant  
63 planets was realised more than 40 years ago<sup>1</sup>, and has since been termed the giant planet  
64 'energy crisis'<sup>2,4</sup>. At Jupiter, only the observed temperatures within the auroral regions  
65 have been adequately explained, as the 1000 - 1400 K temperatures<sup>14</sup> observed there  
66 result from auroral heating mechanisms that impart 200 GW of power per hemisphere  
67 through ion-neutral collisions and Joule heating<sup>15,16</sup>. The low- to mid-latitudes do not have  
68 such a heat source, and yet are measured to be near 800 K, which is 600 K warmer than  
69 can be accounted for by solar heating<sup>15,17</sup>. If heating does not come from above (solar  
70 heating), and cannot be produced in situ via magnetospheric interactions, then a solution  
71 is likely to be found below. Gravity waves, generated in the lower atmosphere and  
72 breaking in the thermosphere, represent a potentially viable source of upper-atmospheric  
73 heating. Previous modelling studies, however, have led to inconclusive results at Jupiter:  
74 while viscous dissipation of gravity waves in Jupiter's upper atmosphere can lead to  
75 warming on the order of 10 K, sensible heat flux divergence can also lead to cooling by a  
76 similar amount, depending on the properties of the wave<sup>6,7</sup>. Recent re-analysis of Galileo  
77 Probe data has shown that gravity waves impart a negligible amount of heating vertically  
78 to the stratosphere (gravity wave motion is primarily longitudinal/latitudinal) and that  
79 heating near the thermosphere is less than 1 K per Jovian day<sup>18</sup>. A more likely energy  
80 source is acoustic waves that heat from below (also via viscous dissipation); this form of  
81 heating requires vertical propagation of disturbances in the low-altitude atmosphere.  
82 Acoustic waves are produced above thunderstorms, and the subsequent waves have been  
83 modelled to heat the upper atmosphere by 10 K per day<sup>19</sup> and observed to heat the  
84 thermosphere over the Andes mountains<sup>19,20</sup>. At Jupiter, acoustic wave heating has been  
85 modelled to potentially impart hundreds of degrees of heating to the upper atmosphere<sup>21</sup>.  
86 However, to date and to the best of our knowledge, no such coupling between the lower  
87 and upper atmosphere has ever been directly observed at the outer planets, so vertical  
88 coupling has not been seriously considered as a solution to the giant planet energy crisis.

89  
90  
91 Jupiter's red spot is the largest storm in the solar system, spanning 22,000 by 12,000 km  
92 in longitude and latitude, respectively. The spot lies within the troposphere, with cloud tops  
93 reaching altitudes of 50 km, around 800 km below the  $H_3^+$  layer<sup>9</sup>. Here we show in Fig. 3.  
94 (as red circles) that the pattern of  $H_3^+$  intensity seen above the spot, when fitted to our  
95 model, gives column averaged  $H_3^+$  temperatures of over 1600 K, higher than anywhere  
96 else on the planet, even in the auroral region. We also fitted temperatures to a swath of  
97 longitudes away from the spot in order to illustrate that the enhancement in temperature  
98 only occurs within this longitude band. The latitudinal variation of temperatures away from  
99 the spot is similar to the ranges previously observed<sup>17</sup>, indicating that the high temperature  
100 above the spot is highly localised in both latitude and longitude.

101  
102  
103 The high temperature in the northern part of the spot provides direct observational  
104 evidence of a localised heating process. We interpret the cause of this heating to be

105 storm-enhanced atmospheric turbulence, which arises due to the flow-shear between the  
106 storm and surrounding atmosphere. A portion of these waves must then propagate  
107 vertically upwards, depositing their energy as heat through viscous dissipation. It is  
108 unknown, at present, why the two red data points at GRS latitudes (grey shaded region in  
109 Fig. 3) differ by 800 K. A possible observational reason could be contamination the  $H_3^+$  line  
110 at 3.45  $\mu\text{m}$  by methane emission line at the same wavelength. Any additional intensity  
111 added to this  $H_3^+$  line results in a lower temperature (for further detail see the Methods  
112 section). Thus, the southern red spot temperature may be much higher than derived, but  
113 only if methane is preferentially brighter in the south. However, as the  $H_3^+$  and  $CH_4$  lines at  
114 3.54 micron are not separated spectrally in this work, it is not possible to conclude whether  
115 or not contamination is present. An alternative physical explanation may relate to the  
116 relative velocities between the zonal wind and the spot being greatest on the equatorward  
117 side of the storm: relative velocities are 75 m/s in the north, 15 m/s in the storm core, and  
118 25 m/s at the poleward edge<sup>9</sup>. The largest relative velocities would induce the strongest  
119 flow shear, leading to the greatest turbulence and therefore the largest contribution to  
120 heating above. It is possible that some signature of such a lower-to-upper atmosphere  
121 energy transfer would be deposited en route in the intervening troposphere and upper-  
122 stratosphere (0 - 150 km altitude, respectively), as there is a 10 K temperature  
123 enhancement encircling the spot at these altitudes<sup>22,23</sup>. However, these enhancements  
124 could also be due to the upwelling of material in the center of the storm, followed by  
125 increased adiabatic heating when the material downwells around the edges<sup>23</sup>.

126  
127

128 The only previous map of Jovian  $H_3^+$  temperatures that contains the spot was made using  
129 ground-based data in 1993<sup>17</sup>. The authors of that study did not mention the GRS, as no  
130 obvious signature was present in their temperature map. However, based on their  
131 contours and the expected red spot location at the time, we estimate that there was a  
132 measured temperature enhancement of 50 K above the spot. While such a minor  
133 temperature increase may indicate that the GRS-driven heating of Jupiter's upper  
134 atmosphere is transient in nature, the spatial resolution of the 1993 observations was 9800  
135 km per pixel (at the equator), compared with 500 km per pixel in this study. Thus the  
136 previous data had significantly cruder resolution in latitude and longitude. The high  
137 temperature region above the spot is localised in latitude in the present work, indicating a  
138 large temperature gradient and perhaps a confinement by presently unknown upper-  
139 atmospheric dynamics. If wave heating driven from below is responsible for the observed  
140 temperatures in Jupiter's non-auroral upper atmosphere, then we might expect a relatively  
141 smooth temperature profile with latitude, punctuated by temperature enhancements above  
142 active storms. The red spot may then simply be the 'smoking gun' that dramatically  
143 demonstrates this atmospheric coupling process, and provides the clue to solving the giant  
144 planet energy crisis.

145

146

147

## References

148

149

150

151

152

153

154

155

156

1. Strobel, D. F. & Smith, G. R. On the temperature of the Jovian thermosphere. *J. Atmos. Sci.* **30**, 718-725 (1973).
2. Miller, S., Aylward, A. & Millward, G. Giant Planet Ionospheres and Thermospheres: The Importance of Ion-Neutral Coupling. *Space Sci. Series of ISSI* **116**, 319-343 (2005).
3. Smith, C. G. A., Aylward, A. D., Millward, G. H., Miller, S. & Moore, L. E. An unexpected cooling effect in Saturn's upper atmosphere. *Nature* **445**, 399-401 (2007).

157

158 4. Yates, J. N., Achilleos, N. & Guio, P. Response of the Jovian thermosphere to a  
159 transient pulse in solar wind pressure. *Planet. Space Sci.* **91**, 27-44 (2014).

160

161 5. Smith, C. G. A. & Aylward, A. D. Coupled rotational dynamics of Jupiter's  
162 thermosphere and magnetosphere. *Annales Geophysicae* **27**, 199-230 (2009).

163

164 6. Hickey, M. P., Walterscheid, R. L. & Schubert, G. Gravity Wave Heating and Cooling in  
165 Jupiter's Thermosphere. *Icarus* **148**, 266-281 (2000).

166

167 7. Matcheva, K. I. & Strobel, D. F. Heating of Jupiter's Thermosphere by Dissipation of  
168 Gravity Waves Due to Molecular Viscosity and Heat Conduction. *Icarus* **140**, 328-340  
169 (1999).

170

171 8. Rayner, J. T. et al. SpeX: A Medium-Resolution 0.8-5.5 Micron Spectrograph and  
172 Imager for the NASA Infrared Telescope Facility. *Publ. Astron. Soc. Pac.* **115**, 362-382  
173 (2003).

174

175 9. Parisi, M., Galanti, E., Finocchiaro, S., Iess, L. & Kaspi, Y. Probing the depth of  
176 Jupiter's Great Red Spot with the Juno gravity experiment. *Icarus* **267**, 232-242 (2016).

177

178 10. Melin, H., Miller, S., Stallard, T., Smith, C. & Grodent, D. Estimated energy balance in  
179 the jovian upper atmosphere during an auroral heating event. *Icarus* **181**, 256-265  
180 (2006).

181

182 11. O'Donoghue, J. et al. Conjugate observations of Saturn's northern and southern  $H_3^+$   
183 aurorae. *Icarus* **229**, 214-220 (2014).

184

185 12. Uno, T. et al. Vertical emissivity profiles of Jupiter's northern  $H_3^+$  and  $H_2$  infrared  
186 auroras observed by Subaru/IRCS. *J. Geophys. Res.* **119**, 10,219-10,241 (2014).

187

188 13. Miller, S., Stallard, T., Smith, C. & et al.  $H_3^+$ : the driver of giant planet atmospheres.  
189 *Phil. Trans. Roy. Soc. London.* **364**, 3121-3137 (2006).

190

191 14. Lystrup, M. B., Miller, S., Dello Russo, N., Vervack, R. J., Jr. & Stallard, T. First Vertical  
192 Ion Density Profile in Jupiter's Auroral Atmosphere: Direct Observations using the Keck  
193 II Telescope. *Astrophys. J.* **677**, 790-797 (2008).

194

195 15. Yelle, R. V. & Miller, S. Jupiter's thermosphere and ionosphere, 185-218 (Cambridge  
196 University Press, 2004).

197

198 16. Cowley, S. W. H. et al. A simple axisymmetric model of magnetosphere-ionosphere  
199 coupling currents in Jupiter's polar ionosphere. *J. Geophys. Res.* **110**, 11209 (2005).

200

201 17. Lam, H. A. et al. A Baseline Spectroscopic Study of the Infrared Auroras of Jupiter.  
202 *Icarus* **127**, 379-393 (1997).

203

204 18. Watkins, C. & Cho, J. Y.-K. The vertical structure of Jupiter's equatorial zonal wind  
205 above the cloud deck, derived using mesoscale gravity waves. *Geophys. Res. Lett.* **40**,  
206 472-476 (2013).

207

- 208 19. Hickey, M. P., Schubert, G. & Walterscheid, R. L. Acoustic wave heating of the  
209 thermosphere. *J. Geophys. Res.* **106**, 21543-21548 (2001).  
210
- 211 20. Walterscheid, R. L., Schubert, G. & Brinkman, D. G. Acoustic waves in the upper  
212 mesosphere and lower thermosphere generated by deep tropical convection. *J.*  
213 *Geophys. Res.* **108**, 1392 (2003).  
214
- 215 21. Schubert, G., Hickey, M. P. & Walterscheid, R. L. Heating of Jupiter's thermosphere by  
216 the dissipation of upward propagating acoustic waves. *Icarus* **163**, 398-413 (2003).  
217
- 218 22. Flasar, F. M. et al. Thermal structure and dynamics of the Jovian atmosphere. I - The  
219 Great Red SPOT. *J. Geophys. Res.* **86**, 8759-8767 (1981).  
220
- 221 23. Fletcher, L. N. et al. Thermal structure and composition of Jupiter's Great Red Spot  
222 from high-resolution thermal imaging. *Icarus* **208**, 306-328 (2010).  
223  
224

### 225 **Acknowledgements**

226 Visiting Astronomer at the Infrared Telescope Facility, which is operated by the University  
227 of Hawaii under contract NNH14CK55B with the National Aeronautics and Space  
228 Administration (NASA). We are grateful to the observing staff at IRTF and Mauna Kea  
229 Observatory for their hard work. This work was funded by NASA under Grant No.  
230 9500303356 issued through the Planetary Astronomy Program for L.M. and J.O'D. The UK  
231 Science and Technology Facilities Council (STFC) supported this work through the  
232 Studentship Enhancement Programme (STEP) for J.O'D, and consolidated grant support  
233 for T.S.S. and H.M (ST/N000749/1). The Royal Astronomical Society partially funded  
234 travel to take the observations. We are grateful for the planetary ephemerides that were  
235 provided by the Planetary Data System.  
236

### 237 **Author contributions**

238 J.O'D. collected, analysed and interpreted the data and wrote the paper. L.M. greatly  
239 assisted in the data reduction, analysis, interpretation and writing of the paper. T.S. helped  
240 with the analysis and interpretation of the data. H.M. assisted in the collection and  
241 reduction of data, and provided computer code necessary for the analysis of data. All  
242 authors provided comments on the manuscript.  
243

### 244 **Author information**

245 Reprints and permissions information is available at [www.nature.com/reprints](http://www.nature.com/reprints). The authors  
246 declare no competing financial interests: details accompany the full-text HTML version of  
247 the paper at [www.nature.com/nature](http://www.nature.com/nature). Correspondence and requests for data and  
248 information should be addressed to JO'D ([jameso@bu.edu](mailto:jameso@bu.edu)).  
249  
250  
251  
252  
253  
254  
255  
256  
257  
258  
259

260  
261  
262  
263  
264  
265  
266  
267  
268  
269  
270  
271  
272  
273  
274  
275  
276  
277  
278  
279  
280  
281  
282  
283  
284  
285  
286  
287  
288  
289  
290  
291  
292  
293  
294  
295  
296  
297  
298  
299  
300  
301  
302  
303  
304  
305  
306  
307  
308  
309  
310  
311

**Figure 1.** The acquisition of Jovian spectra. In **a** we show Jupiter as observed by the SpeX slit-jaw imager and L-filter (3.13 - 3.53  $\mu\text{m}$ ), on 4 December 2012. Bright regions at the poles result from auroral emissions; the contrast at low- and mid-latitudes has been enhanced for visibility. The vertical beige line in the middle of the image indicates the position of the spectrometer slit, which was aligned along the rotational axis. In **b** we show the co-added spectrum of seven GRS-containing exposures; dotted horizontal lines indicate the latitudinal range of the spot. Further details are given in the Methods section.

**Figure 2.** Model fit to observed  $\text{H}_3^+$  intensity as a function of wavelength. **a** is produced from the data in Fig. 1**b** between  $-13^\circ$  and  $-19^\circ$  planetocentric latitude, while **b** corresponds to  $-40^\circ$  and  $-49^\circ$  latitude. The model fit to the data is shown in solid red: only the  $\text{H}_3^+$  lines at 3.383  $\mu\text{m}$  and 3.454  $\mu\text{m}$  are included in the temperature derivation (see Methods for the full list). Telluric absorption, normalised to show sky contamination, is shown in grey. The derived temperatures are **a**  $1644 \pm 161$  K and **b**  $900 \pm 42$  K (standard errors). The  $\text{H}_3^+$  model is extended to the central region (dashed red) based on the temperatures and densities of the fits. Intensity errors are 1-sigma.

**Figure 3.** Jovian  $\text{H}_3^+$  temperatures versus planetocentric latitude. Column-averaged temperatures of  $\text{H}_3^+$  shown here are each derived from model fits to the discrete  $\text{H}_3^+$  emission lines as shown in Fig. 2. Red circles correspond to the co-add of GRS spectra between 239 - 253 degrees system III Central Meridian Longitude (CML) shown in Fig. 1**b**. The blue triangled data was derived from exposures taken between 293 - 359 and 0 - 82 degrees CML - i.e. longitudes well separated from the spot, representing the 'ordinary' background conditions based on solar heating alone. The modelled temperature of the upper atmosphere for these non-auroral regions is 203 K<sup>1</sup>. Uncertainties are standard error on the mean.

312  
313  
314  
315  
316  
317  
318  
319  
320  
321  
322  
323  
324  
325  
326  
327  
328  
329  
330  
331  
332  
333  
334  
335  
336  
337  
338  
339  
340  
341  
342  
343  
344  
345  
346  
347  
348  
349  
350  
351  
352  
353  
354  
355  
356  
357  
358  
359  
360  
361  
362  
363

## Methods

**Additional observing details.** In Fig. 1, where we show the acquisition of Jovian spectra, Jupiter's sub-Earth latitude was +3 degrees. The configuration of the SpeX instrument on the IRTF was single order with a long slit, at a spectral resolution of  $R = 2,500$ . The slit length and width used was 60 and 0.3 arc seconds, respectively, and one pixel subtended 0.15 arc seconds on the sky. In Fig. 2 the model telluric transmission spectrum is obtained from the Atmospheric TRANsmission database (ATRAN; <https://atran.sofia.usra.edu>) for a spectral resolution of  $R = 2,500$ . The absorption wells near  $H_3^+$  lines in the center of the spectrum in Fig. 2 serve to highlight our reasons for avoiding that region in the temperature fitting. The attenuation of the signal in this figure by the sky is constant as a function of latitude because all of the temperature fits are from the same exposure, so any attenuation would affect each temperature as a function of latitude in the same way.

**Absolute calibration.** We flux calibrated the data by using the photometric-standard AOV star HR1019 in the usual manner: i.e., by assuming a blackbody curve for the temperature of the star (10,000 K - in this case) and comparing it to what we observed. This is dual-purpose in that by dividing the data by the flux calibration, it converts counts into physical units of flux and also yields a profile of what the sky has absorbed. The mean uncertainty in the absolute calibration as a function of wavelength is 4% of the flux, and the S/N for the star was 24.

**Instrumental effects.** These are accounted for by flat fielding, dark-current subtraction and hot pixel removal in every frame. The calibrated Jovian spectra (containing uncertainties in absolute calibration above) also include noise from the instrumentation and Earth's atmospheric attenuation. The uncertainties are thus found by finding the standard deviation of the backgrounds in the final spectrum. All errors are propagated through with the absolute calibration and uncertainty to produce the error bars in intensity displayed in Fig. 2 and the temperature estimates in Fig. 3.

**$H_3^+$  fitting.** In order to find the temperatures from Fig. 1b, we used a spectroscopic  $H_3^+$  line list<sup>24</sup> and the most recent  $H_3^+$  partition function coefficients<sup>25</sup>. The spectrum of  $H_3^+$  can be treated as a sum of Gaussian distribution curves, with each curve a function of temperature. This 'equation of a spectrum' is solved in order to derive the temperature<sup>26</sup>. This technique has been used to derive  $H_3^+$  temperatures at Jupiter, Saturn, and Uranus for decades<sup>27</sup>, with typical uncertainties of 10%. The fitting routines used are the same as those in previous literature<sup>26</sup>, and include a list of over 3 million ro-vibrational transition lines of  $H_3^+$ <sup>24</sup>. The fitting routine uses the most recent partition function constants to establish a temperature, which are applicable for temperatures between 100 and 10,000 K (whereupon the ion dissociates)<sup>25</sup>.

**Handling of non- $H_3^+$  intensity.** We now address the possibility of attenuation of  $H_3^+$  by other sources at Jupiter. Possibility 1 is that there is enhanced reflection of sunlight from haze at the red spot location, but this is not seen adjacent in wavelength to any lines in Fig. 1 and can consequently be ruled out. Possibility 2 pertains to emission from neutral gases. Only the two intensity peaks overlain with solid red lines are included in the final fit, though the left peak contained the  $H_3$  lines at 3.38285  $\mu\text{m}$  and 3.38391  $\mu\text{m}$ , whereas the right peak line included 3.45502  $\mu\text{m}$ , 3.45483  $\mu\text{m}$  and 3.45468  $\mu\text{m}$ . Methane ( $\text{CH}_4$ ), the dominant hydrocarbon in Jupiter's atmosphere, is known to emit at a number of

364 wavelengths in this region, namely 3.380  $\mu\text{m}$ , 3.392  $\mu\text{m}$ , 3.404  $\mu\text{m}$ , 3.415  $\mu\text{m}$ , 3.440  $\mu\text{m}$   
365 and 3.454  $\mu\text{m}$ . Some of these are visible in Fig. 1 (e.g. 3.404  $\mu\text{m}$ ) and some are not (e.g.  
366 3.380  $\mu\text{m}$ ), but we are mainly interested in any that could affect the fitted  $\text{H}_3^+$ , which means  
367 ignoring for now the central portion of Fig. 2. The  $\text{CH}_4$  emission line at 3.454  $\mu\text{m}$  is the only  
368 line that could possibly fall on a fitted  $\text{H}_3^+$  line, and the effect of it doing so would mean that  
369 the line ratio between the  $\text{H}_3^+$  lines denoted by solid-red fit would be larger. For this  
370 particular set of lines, if the ratio is increased, then the temperature estimate decreases:  
371 this can be seen by comparing the ratios of lines in Fig. 2, with the lower ratio GRS  
372 spectrum corresponding to 1644 K  $\pm$ 161 K, while the higher ratio non-GRS spectrum is  
373 fitted as 900  $\pm$ 42 K (s.e.m). In other words, if methane was contributing emission to this  
374 line, then accounting for it in some way by removing an arbitrary amount would result in  
375 the GRS temperature fitted being even higher than the 1600 K derived here.

376  
377 **Code availability.** The  $\text{H}_3^+$  spectroscopic line list used in the model is available online at  
378 [www.exomol.com/data/molecules](http://www.exomol.com/data/molecules), in addition, an online  $\text{H}_3^+$  intensity calculator is available  
379 at <http://h3plus.uiuc.edu>. The model fitting routines and reduction code used in this work is  
380 available on request ([jameso@bu.edu](mailto:jameso@bu.edu)). Our data reduction pipeline makes substantial use  
381 of the NASA Astronomy IDL library, available online at <http://idlastro.gsfc.nasa.gov>.

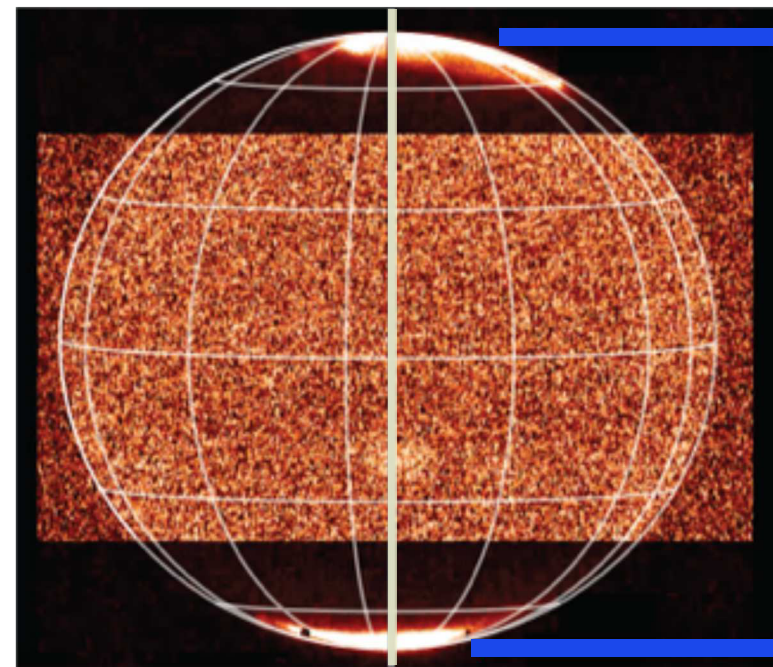
#### 382 383 384 **Additional references**

385 24. Neale, L., Miller, S. & Tennyson, J. Spectroscopic Properties of the  $\text{H}_3^+$  Molecule: A  
386 New Calculated Line List. *Astrophys. J.* **464**, 516-520 (1996).

387  
388 25. Miller, S., Stallard, T., Melin, H. & Tennyson, J.  $\text{H}_3^+$  cooling in planetary atmospheres.  
389 *Faraday Discussions* **147**, 283-291 (2010).

390  
391 26. Melin, H. et al. On the anticorrelation between  $\text{H}_3^+$  temperature and density in giant  
392 planet ionospheres. *Mon. Not. R. Astron. Soc.* **438**, 1611-1617 (2014).

393  
394 27. Stallard, T. S. et al. Temperature changes and energy inputs in giant planet  
395 atmospheres: what we are learning from  $\text{H}_3^+$ . *Phil. Trans. Roy. Soc.* **370**, 5213-5224  
396 (2012).

**a****b**